High resolution small-scale inorganic scintillator detector: HDR brachytherapy application

Sree Bash Chandra Debnath, Marjorie Ferre, Didier Tonneau, Carole Fauquet,
Agnes Tallet, Anthony Goncalves, Julien Darreon

High resolution small-scale inorganic scintillator detector: HDR brachytherapy application

S.B.C. DEBNATH[1*], M. FERRE[2], D. TONNEAU[1], C. FAUQUET [1], A. TALLET[2], A. GONCALVES[2,3], J. DARREON [2]

[1]Aix Marseille Université, CNRS, CINaM UMR 7325, 13288, Marseille, France

[2]Institut Paoli-Calmettes, 13009, Marseille, France

[3]Aix Marseille Université, CNRS UMR 7258, INSERM UMR 1068, CRCM, 13009 Marseille, France

Abstract

Purpose: Brachytherapy (BT) deals with high gradient internal dose irradiation made up of a complex system where the source is placed nearby the tumor to destroy cancerous cells. A primary concern of clinical safety in BT is quality assurance to ensure the best matches between the delivered and prescribed doses targeting small volume tumors and sparing surrounding healthy tissues. Hence, the purpose of this study is to evaluate the performance of a point size inorganic scintillator detector (ISD) in terms of high dose rate brachytherapy (HDR-BT) treatment.

Methods: A prototype of the dose verification system has been developed based on scintillating dosimetry to measure a high dose rate while using an ^{192}Ir BT source. The associated dose rate is measured in photons/s employing a highly sensitive photon counter (design data: 20 photons/s). Dose measurement was performed as a function of source-to-detector distance according to TG43U1 recommendations. Overall measurements were carried out inside water phantoms keeping the ISD along the BT needle; a minimum of 0.1 cm distance was maintained between each measurement point. The planned dwell times were measured accurately from the difference of two adjacent times of transit. The ISD system performances were also evaluated in terms of dose linearity, energy dependency, scintillation stability, signal-to-noise ratio (SNR), and signal-to-background ratio (SBR). Finally, a comparison was presented between the ISD measurements and results obtained from TG43 reference dataset.

Results: The detection efficiency of the ISD was verified by measuring the planned dwell times at different dwell positions. Measurements demonstrated that the ISD has a perfectly linear behavior with dose rate (R^2=1) and shows high SNR (>35) and SBR (>36) values even at the lowest dose rate investigated at around 10 cm from the source. Standard deviation (1σ) remains within 0.03% of signal magnitude, and less than 0.01% STEM signal was monitored at 0.1cm source-to-detector distance. Stability of 0.54% is achieved, and afterglow stays less than 1% of the

total signal in all the irradiations. Excellent symmetrical behavior of the dose rate regarding source position was observed at different radiation planes. Finally, a comparison with TG-43 reference dataset shows that corrected measurements agreed with simulation data within 1.2% and 1.3%, and valid for the source-to-detector distance greater than 0.25 cm.

40 **Conclusion:** The proposed ISD in this study anticipated that the system could be promoted to validate with further clinical investigations. It allows an appropriate dose verification with dwell-time estimation during source tracking and suitable dose measurement with a high spatial resolution both nearby (high dose gradient) and far (low dose gradient) from the source position.

45 **1 Introduction**

Brachytherapy (BT) refers to a High Dose Rate (HDR), Low Dose Rate (LDR) or Pulsed Dose Rate (PDR) treatment technique. In contrast to external beam radiotherapy, this technique requires internal high dose gradient *in-vivo* dosimetry that can lead to several errors. All these errors are 50 still unnoticed due to the conventional complex procedures applied in BT[1-4]. Hence, a significant deviation is commonly observed between planned and measured dose in the region of interest [5-9]. Appropriate dose measurement remains very challenging to conform with the quality assurance of the treatment plan.

High deviation of the measured dose can be observed for a few millimeters of displacement in the 55 steep dose gradients zone (e.g., near the source) that limits the *in-vivo* dosimetry (IVD) in BT using large sensitive volume conventional dosimeters. To perform the source tracking, millimeter precision in the dwell positions is needed as reported by several research groups [10-14]. Any small offset in these parameters can distort the dose distribution and leads to errors between planned and delivered dose. Due to the afterloader malfunction, timing incidence could occur in addition to 60 positional errors that can result in a harmful consequence for the patient. Using a point size detector, one can expect a better accuracy in dwell positions and dwell times verification in source tracking during HDR-BT. Indeed, several BT treatment errors can be avoided through the implementation of real-time *in-vivo* dosimetry [2,15,16]. However, considering current technology that is challenging to incorporate in the clinical assignment, BT treatment errors are still overlooked 65 for long periods [2,4,17-19]. Therefore, an accurate, precise, and straightforward real-time dose verification technology could reduce the risk of errors and improve the patient safety during HDR-BT treatment.

Fiber based scintillating dosimetry system that consists of scintillating materials coupled to the optical fiber apex has already been used in different high energy radiation measurements [20-23]. The 70 scintillator-based detector was proposed by several research groups and can be useful to measure the step dose gradient nearby the tumor in the case of BT treatment [15,24-26]. Scintillators used in those dosimeters can be organic or inorganic. These reduced size detectors can mitigate the issue of volume averaging effect and can facilitate the accurate dose measurement in the tumor region and identify the treatment error [14,15,27]. Due to the size of these detectors, they can easily be fitted

75   through BT catheters hence can be particularly suitable for real-time *in-vivo* dose measurement during BT [14,24-26].

Despite the aforementioned advantages, the major issue of using these scintillating detectors is stem effect, induced in the fiber, a combination of Cerenkov and fiber excited luminescence when large core plastic fiber is irradiated [20,22,28,29]. This effect is also related to the exposed volume of
80   the detector, and fiber used in the detector. Indeed, conventional detectors require a significant volume of scintillators and optical fiber cable to detect and transmit the scintillating signal. So, stem effect contribution must be extracted from the total detected signal. Though several removal techniques [23,30,31] have already been proposed to reduce this parasitic effect, these dosimeters are still subject to correction due to the lower scintillation signal induced by a minimum scintillating
85   volume required to be used in BT. Therefore, an efficient scintillator that could provide higher signal intensity is essential to achieve significant scintillating intensities compared to the stem effect generation in the fiber.

Owing to the eminent luminescence yields, inorganic scintillators demonstrate scintillation intensities much higher than plastic scintillators implemented in some recent works [32,33]. Such
90   properties can reduce the relative influence of stem contribution in photoluminescence signal and have shown promise to be used in BT [34,35]. More specifically, recent studies highlighted the interest of five inorganic scintillators (ruby (Al_2O_3:Cr), Y_2O_3:Eu, YVO_4:Eu, ZnSe:O and CsI:Tl) [32], and have shown that ZnSe:O exhibits the most favorable characteristics to be used in BT. However, the average scintillating volume used in this study was around 10^{-3} cm^3, which may introduce a
95   parasitic convolution effect in dose distribution profiles. Moreover, some scintillators used in this research work have shown unstable scintillating intensity, significant afterglow, and require significant energy, temperature[36], and fiber signal attenuation corrections.

In this context, this work is focused on the performance evaluation of a small-scale inorganic scintillator detector (ISD) to characterize HDR-BT source in terms of several dosimetric
100 characteristics. The detector used is based on (Zn,Cd)S:Ag inorganic scintillating material selected due to its eminent luminescence properties obtained even with a minimum volume. Overall measurements were performed both in solid water phantoms and IBA^{TM} water tank phantoms to estimate the measurement accuracy. The ISD was used to accurately measure planned dwell times of the ^{192}Ir source coming from a remotely controlled afterloader BT machine. Dosimetric
105 characteristics such as linearity, repeatability, scintillator stability, Signal-to-Noise ratio (SNR), and Signal-to-Background (SBR) were studied. Finally, a comparison was shown between the ISD measurements and results obtained from TG-43 reference dataset.

2   Materials and methods

110 ### 2.1   Sensor preparation and system characteristics

The scintillating detector used was made of 10 m silica (SiO_2) optical fiber coupled with (Zn,Cd)S:Ag scintillating materials at the fiber apex. The optical fiber core, cladding, and outer coating were 50 μm, 125 μm, and 250 μm respectively, whereas the bandwidth of the fiber remained in 400-2100 nm. The scintillating material (ref. JGL47/S-R1) was provided by 'Phosphor

115 Technology®' and the fiber (ref. FG050UGA) was provided by Thorlabs™. According to the technique, already detailed in [20], fiber clipping, apex testing, grafting technique (PMMA resist diluted in Ethyl lactate ($C_5H_{10}O_3$) solvent used), and fabrication of the ISD was studied to develop the fiber integrated inorganic detector. After fabricating the ISD with (Zn,Cd)S:Ag scintillating materials, the estimated scintillating volume of the detector is 2.9×10^{-9} cm^3. Due to the eminent

120 luminescence properties, this small volume was sufficient to achieve a significant output signal. Note that, (Zn,Cd)S:Ag scintillator was chosen due to its efficient red emission tested under low energy BT radiation. The outer diameter of the scintillating head is ~150 μm, hence the detector was sufficiently small to be placed inside the BT needle during the experiment. A photon counter is used to measure output luminescence signal in photons/s, which is associated with the dose rate.

125 Photon counter (ref. SPD_A_VIS_M1) provided by 'Aurea Technology™, works around its maximum quantum efficiency (~70%) during the detection of visible photons. This device is based on Si-Schottky diode technology.

2.2 Experimental setup and source

All the measurements were performed at the Brachytherapy department of Institute Paoli-

130 Calmettes hospital using an Elekta microSelectron HDR-V2 afterloader with air-kerma strengths 30.8 to 47.45 mGy.m^2.h^{-1} during the experiments. The afterloader is equipped with an Iridium source (^{192}Ir) with an initial activity of 430 GBq. The source characteristics dimensions are as follows: capsule diameter 0.09 cm; length 0.45 cm and source pellet diameter 0.06 cm; length 0.35 cm, respectively. Irradiation times are given as nominal second. Based on the afterloader user

135 manual, the source position is specified within ±0.05 cm accuracy.

According to the measurement requirements, two different setups (water tank phantoms and solid water phantoms) have been used. The water tank phantoms set-up is shown in **Fig**. 1 (a). The phantom system used is an IBA^{TM} blue phantom with external dimensions of 67.5 x 64.5 x 56 cm^3 that allows dose distribution measurements in arbitrary in-depth horizontal planes with high

140 precision according to international standards (IAEA, AAPM, etc.). This blue phantom system uses non-contact position sensor technology equipped with a 3-axis translation stage comprises a scanning volume of 48 x 48 x 41 cm^3 with a positional accuracy of ± 0.01 cm. **Fig**. 1(b) shows a schematic representation of the whole set-up to realize the ISD head position and relevant critical distances. In the scanning unit, the ISD head is positioned in the horizontal plane, and the fiber

145 axis remains along the Y-axis, perpendicular to the source catheter. In this case, the source is fixed while the detector moves by means of the translation stage. Therefore, the source catheter is attached to the tank wall at a depth Z, chosen as reference Z = 0 plane. The ISD head was moved along the radial distance (e.g., X-axis) at different Z-planes to measure the dose rate at different source-to-detector distances.
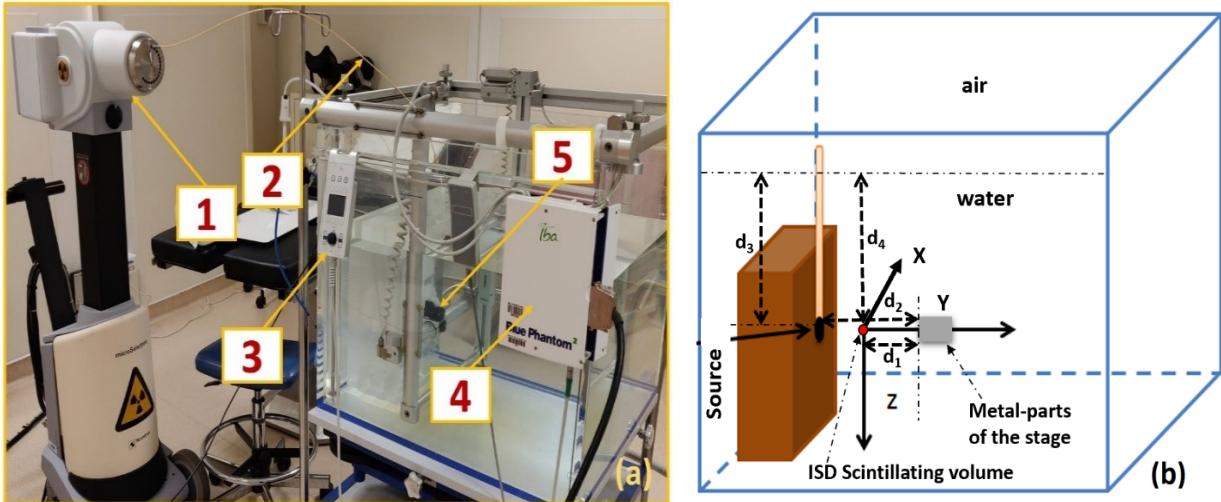
Fig. 1 (a) Experimental setup for testing HDR BT under 3D water phantom system. (1) MicroSelectron HDR afterloader unit (2) Catheter (3) Position controller (4) IBA^{TM} Electronics board for remote control (5) Motor scanner (3-axis translation stage). (b) A scheme (side view) of the experimental setup highlighting the critical distances. d_1:closest distance between scintillating volume and metal parts of the stage=1.5 cm; d_2:closest distance between source positions and metal parts of the stage =1.7 cm; d_3:closest distance between source position and air =30 cm; d_4:closest distance between scintillating volume and air = 20 cm.

Fig. 2 shows the solid water phantom set-up particularly dedicated to dwell time measurements. Several catheters that are coming out from the afterloader can be simultaneously connected and different needles were used to place the source and the detector inside the catheters. The detector was placed inside one of the needles through a catheter tube whereas the source can move inside other needles of the prescribed channels. Catheters are sandwiched between solid water equivalent slabs, where red markers identify the planned source dwell positions (**Fig**. 2(b)).
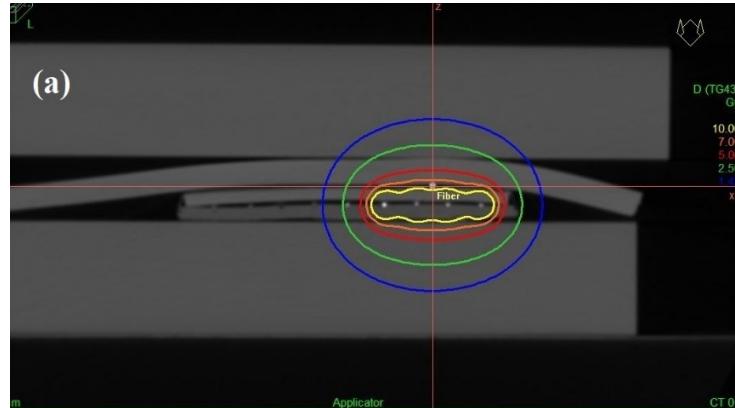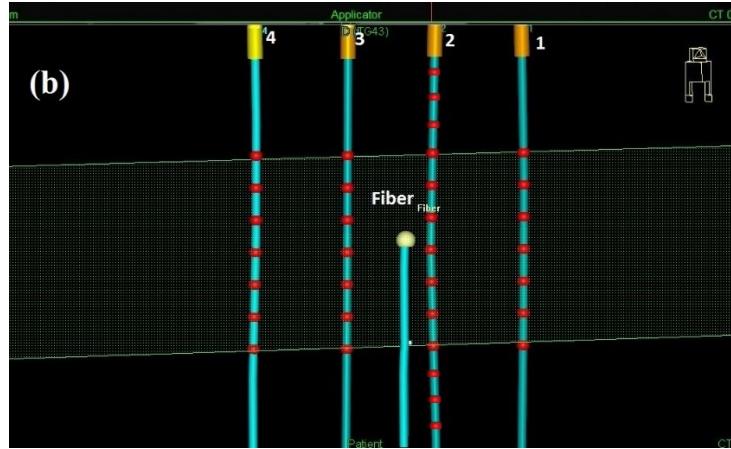
Fig. 2: a) Front view of the solid water phantom setup showing the source catheters and the ISD sensitive head sandwiched between solid water slabs. (b) System top view showing dwell positions of the source (red markers) through different catheter tubes (1, 2, 3, and 4) inside solid phantoms. ISD carrying catheter (no markers) placed in between source catheters, where the ISD sensitive head is represented by a big white spot.

2.3 Dwell time measurement

Dwell time measurements were carried out using solid water phantom placed on the patient couch to precisely calculate the dwell time for different dwell positions. In this case, a CT-scan was initially performed before BT testing to track the initial position of the source catheters and the detector, as shown in **Fig**. 2**.** During irradiation, the radioactive source position was planned along the catheter tube to achieve the desired dwell positions while the ISD was maintained at a fixed position. X and Z positions are chosen at 5.1 cm and -2.0 cm, while Y was varied between -2.44 cm to -5.44 cm by steps of 0.25 cm. When the source moved between two dwell positions, the 'time of transit' was recorded using the difference in photon rate between two measurements. Then, dwell times were measured by the ISD from the difference of two adjacent time of transit. The dwell times at different dwell positions was varied to check if the ISD is dynamic and sensitive enough to measure the exact planned dwell time at a specified dwell position. The source coordinates, dwell positions, and variation of the planned dwell times for one of the four different catheters (e.g., catheter 2) is shown in **Table** 1. The ISD was tested for detecting these varying dwell times at different dwell positions.

The individual dwell time at each dwell position was calculated by subtracting two successive time instances when a significant dose rate variation is observed (e.g., during transit of source). Thus, we chose to follow the variations with time of the parameter C_i given by[37]-

$$C_i = \frac{S_i - S_{i+1}}{S_i + S_{i+1}} \tag{1}$$

Where C_i is the normalized absolute change in the measurement between two adjacent measurements, S_i is the signal at time t_i. When the source is fixed at a dwell position between t_i and t_{i+1}, ideally, C_i should be zero.

2.4 Scintillation and background signals

The output signal collected by the photon counter is composed of scintillator luminescence signal, the dark noise, and possible stem signal generated by optical fiber. The dark noise can easily be removed from the total signal as it is calibrated and quantified at the beginning of each measurement during the experiment. The stem signal, where a significant portion is coming from the Cerenkov radiation, commonly increases with the fiber irradiated volume [32,38].Note that, this signal is expected to be insignificant due to the small size silica fiber volume irradiated, and as characterized previously[20]. However, a bare fiber was used to quantify the stem signal, so that the exact ISD output signal can be ensured. Thus, the exact scintillation signal generated due to the irradiation is measured by subtracting stem signal and the dark noise from the total signal. Due to very low signal attenuation (30 dB/km) through the optical fiber, the system does not require any corrections for signal transmission loss throughout the fiber [20].

2.5 Stability of scintillation

The constant output signal during several identical irradiations by the BT source refers to the scintillation stability, and the persistence of visible photon emission even after the source retraction refers to afterglow. Both parameters were measured for the ISD following the detailed description given by [32,33]. The scintillating stability was measured when the source was placed to a specified dwell position and afterglow was measured as soon as the source retracted from that position. For this experiment, the ISD was irradiated by the source for three repetitive measurements with 10 minutes pause in between when source-to-detector radial distance was 2 cm. These experiments also allow to check if the scintillation intensity differs beyond any positional uncertainty of the source ($\pm$ 0.05 cm). Note that, scintillation stability was checked prior to any other measurements under BT source irradiation. No corrections were considered for stability and afterglow measurements.

2.6 Dose linearity and repeatability

The linearity of the detector's output signal with respect to the cumulative absorbed dose was tested for different amounts of dose irradiation. For this purpose, the detector was placed at 2 cm and 3 cm distance in the X-coordinate (X= 2, 3cm; Z=0) from the source during the time interval and irradiated with a dose of 0.8 Gy to 6 Gy inside water. Two different positions were chosen to confirm the linearity of the device and system. During each measurement, the time for irradiation was varied, hence total amount of irradiated dose varied accordingly considering the uniform dose rate over the period at that position. The irradiation for 1.5, 3, and 6 Gy was conducted 5 times to verify the repeatability of the measurements. The dose rate was estimated at 28 mGy/s and 12.5 mGy/s respectively for 2 cm and 3 cm distance. The photon counter provides a photon flux signal (in photons/s) whose variations with time were recorded and finally integrated to obtain the optical intensity (total number of photons). Note that, no corrections are required during dose linearity measurement.

2.7 Dose rate measurement (uncorrected)

The ISD was characterized to measure the dose rate available at different distances from the radioactive source and at different azimuths and elevations inside the water tank phantom previously described (section 2.2) to simulate the *in-vivo* case. Ideally, using a point source inside

a spherical capsule, radiation should be isotropic. According to the source geometry, we can assume the source might not be in an ideal case. Therefore, suitable measurements are required to realize the dose distribution pattern of the source. All dose values were calculated according to the AAPM TG-43 protocol as implemented in the software.

235   Note that, scintillation intensity measured by the ISD is assumed to be proportional to the absorbed dose by the scintillating volume. The calibration coefficient for the detector was determined for 1cm radial distance from BT source (X=1 cm, Z=0), where the measured scintillating signal was divided by the data dose at this position provided by TG-43 dataset [39]. This calibration coefficient was used to measure the dose rate at the other distances. Afterward, the dose rate for the ISD was

240   measured for several planned dwell positions displacing between 0 to 10 cm along X-axis at different Z-planes within ±5cm. The source and detector positional uncertainties were given in section 2.2.

The positioning uncertainty dominates in measurements close to the source, whereas measurement uncertainty dominates at long distances as demonstrated by [14]. Therefore, a source dwell time of

245   50 s was used at each position to ensure that we have enough data points in the ISD recorded signal.

2.8   Energy dependence and corrected dose rate

During source irradiation, the absorbed dose effectively depends on the incident photon energy and the effective atomic number (Z_{eff}) of the irradiated medium. The energy spectrum of the BT

250   source in water strongly depends on the distance from the source [40]. As the scintillator ($Z_{eff\,sci}$) used here is not water ($Z_{eff\,water}$) equivalent, the absorbed dose measured in scintillator volume is not the same as in water other than the calibrated position (normalization position X=1 cm, Z=0), which results in the energy dependency of the inorganic detector.

Thus, the energy dependency of the ISD was investigated to calculate the corrected dose rate. This

255   measurement was performed at Z=0 plane, while detector was moved along the radial distance (X-axis) starting from 0.25 cm from the source center inside the water tank. For different source-to-detector distances, the ratio between the ISD and TG-43 dose rate was fitted with a first-order polynomial at Z=0 plane whereas, a 3rd order polynomial was fitted for Z=5 cm plane. These energy correction parameters were used to correct the measured dose rate at the ISD due to its

260   energy dependency inside water.

3 Results

3.1   STEM signal characterizations

STEM signal was measured using the solid water phantom (see system top view Fig.3). A bare

265   fiber and an ISD were sandwiched between 10 cm of solid water slabs at a fixed position. BT source was displaced through a catheter in parallel to bare/ISD fiber, at d=0.5 cm and 0.1 cm source catheter to fiber distances. No scintillating signal was detected during source travel between point A to point C, at d=0.5 cm source catheter-bare fiber distance, hence signal always remained within noise level. When the source catheter is in contact with bare fiber (source catheter to fiber

270   distance ~ 0.1 cm), a STEM signal of 180 photons/s was detected during source travel from point A to point B. After that, this signal came back to the noise level when the source exceeded the bare fiber head position (point B to C). Note that identical measurements have been done using the ISD fiber, and we have found that the STEM signal measured by bare fiber corresponds to less than 0.01% of the total signal collected by the ISD for source position, d=0.1 cm. The parasitic stem

275   signal remains within the dark noise and cannot be quantified for source to detector fiber distances higher than 0.1 cm.
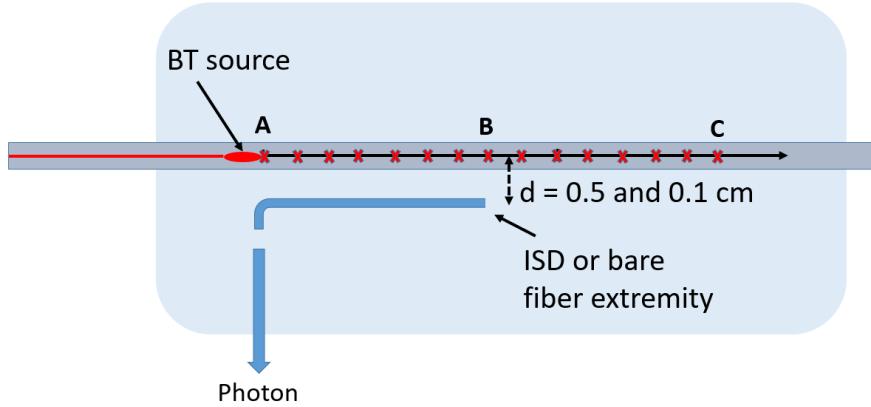

Fig. 3. STEM signal characterizations protocol.

3.2   Dwell time measurement by ISD

280   During ISD irradiation, BT source was planned to stop at different dwell positions inside the source catheter while the optical signal is continuously recorded by the ISD maintained at a fixed position. The measured optical signal variations are shown in **Fig**. 4. The displacement between each dwell position (distance between two successive positions) was 0.25 cm. Dwell time was varied for each dwell position as given in **Table** 1. In this case, the signal increases when the source approached

285   the detector and achieves a maximum value for the minimum source-to-detector distance during the travel. Due to the high sensitivity of the detector, signal magnitude observed at two successive positions can easily be discriminated, which signifies that source displacement can easily be tracked by the ISD.

(a)

(b)
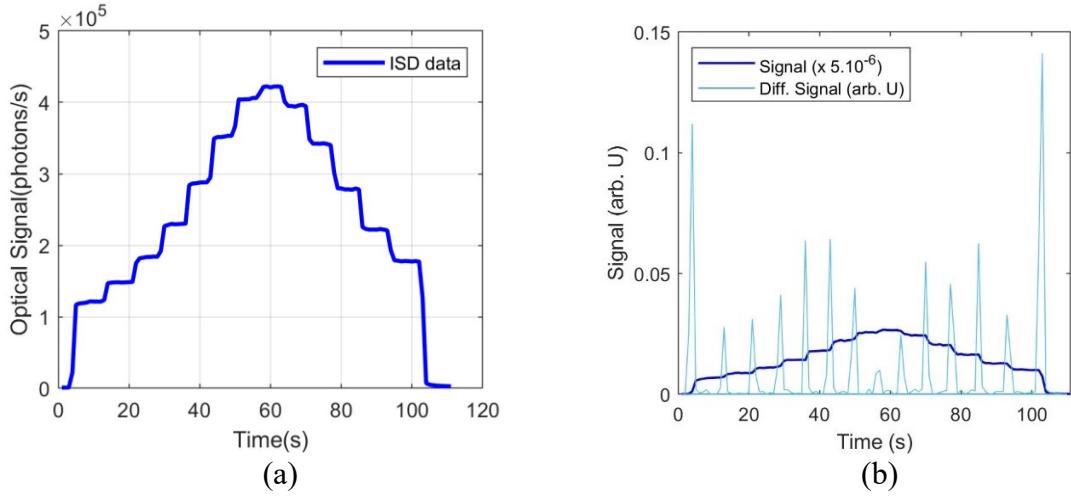
290

Fig. 4: (a) Real-time ISD signal variations with time during BT source travelling through its catheter. The dwell positions varied from -2.44 cm to -5.44 cm by steps of 0.25 cm. Different dwell times were selected (Table 1). (b) difference between two adjacent measurements divided by the sum of the two measurements. Data measurements are shown only for Catheter 2.

295 **Fig**. 4(b) shows the time dependence of C_i (equation 1) during the measurement process. This figure exhibits the sharp peaks each time source is moved between two successive dwell positions, while C_i remains at the dark noise (background) level of 250 ph/s each time the source stays at a dwell position. The separation between two successive peaks corresponds to the ISD exposure time (dwell time), while the peak width is the source transition time between two positions. The

300 measured dwell times were found to be acceptable with the planned dwell time as shown in **Table** 1, and matched with 0.09% average accuracy.

Position	1	2	3	4	5	6	7	8	9	10	11	12	13
Y(cm)	-2.44	-2.69	-2.94	-3.19	-3.44	-3.69	-3.94	-4.19	-4.44	-4.69	-4.94	-5.19	-5.44
Planned Dwell time (s)	9.2	8.3	7.7	7.2	6.9	6.8	6.7	6.8	6.9	7.2	7.6	8.3	9.1
Measured dwell times (s)	9.19	8.29	7.71	7.2	6.88	6.8	6.71	6.8	6.89	7.2	7.59	8.29	9.09
Time difference (s)	0.01	0.01	0.01	0	0.02	0	0.01	0.01	0	0.01	0.01	0.01	0.01
Time difference (%)	0.11	0.12	0.13	0	0.28	0	0.15	0.15	0	0.14	0.13	0.12	0.11
Scintillator-to-source distance(cm)	1.66	1.47	1.31	1.18	1.1	1.04	1.07	1.14	1.27	1.43	1.61	1.8	2.01

Table 1: Dwell time measurements at different dwell positions inside Catheter 2. Source movement step =0.25 cm and total no. of dwell positions =13

3.3 Dose linearity and repeatability

305 **Fig**. 5 shows the optical intensity with respect to the total amount of BT irradiation dose for two different ISD detector positions. The optical intensity is entirely proportional to the dose in both cases. The linear regression analysis in both cases is observed $R^2 =1$, which determines the perfect system linear behavior with respect to the delivered dose. At a dose rate of 28 mGy/s, we found a slope of 1.4×10^7 photons/Gy, while at the dose rate of 12 mGy/s, the slope is 2×10^7 photons/Gy.
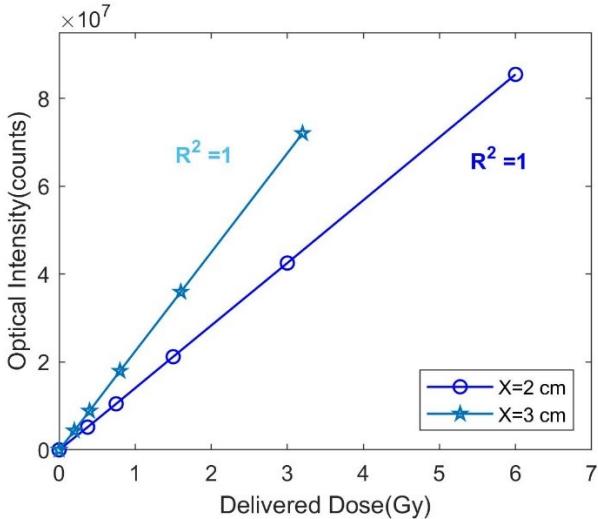
Fig. 5: Linearity of the ISD signal with respect to delivered dose. At X = 2 cm, dose rate is 28 mGy/s and X = 3 cm, dose rate is 12 mGy/s.

The measurement for the repeatability test at each measurement position shows that the ISD variation is less than 0.35% among all the measurements. Therefore, excellent repeatability was obtained.

3.4 Scintillation stability and afterglow

Fig. 6(a) shows the scintillation stability of the ISD for three consecutive 6 Gy dose irradiations delivered at a dose rate of ~28 mGy/s at 2 cm source-to-detector radial distance. As highlighted by this figure, the signal is very stable with time when the source remains at its dwell position. The maximum deviation of the repetitive and consecutive irradiations was found to be 0.54%.

320 The rise-time includes detector stabilization time and source forward transition time, while fall-time considers source transition for removal and scintillator afterglow. **Fig**. 6(b) shows a close view of **Fig**. 6(a) in both linear and logarithmic scales starting from source retraction command, whereas log curve gives better sight of the afterglow. First, the signal rapidly decreases from 100% to 0.2%, when the source is retracted from the catheter. This fall-time stays during 2s, which corresponds to the source retraction time observed when irradiation is stopped. However, the signal decreases slowly from 0.2% to dark noise level during 8 s. This queue signal corresponds to scintillator afterglow and can be a crucial issue in the accurate dose measurement. However, in our case, the afterglow magnitude does not exceed 1% of the maximum signal.
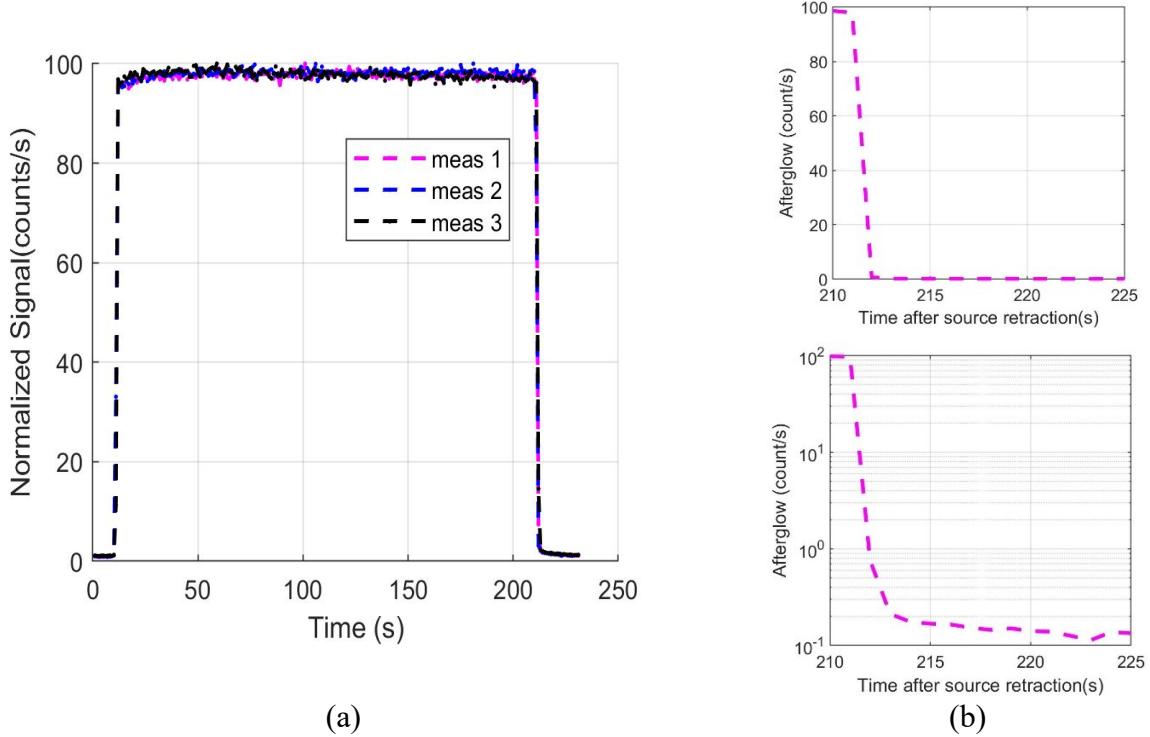
(a)　　　　　　　　　　　　　　　　　　　(b)

Fig. 6: Scintillation stability for (a) repeated BT irradiations and (b) afterglow effect after the source retraction both in linear (upper graph) and logarithmic scale (lower graph).

3.5　Dose rate as a function of distance

The dose rate measurements were carried out by moving the detector along X-axis within different horizontal planes at Z= 0, ±1, ±2, ±3, and ±5 cm, and the corresponding results are shown in **Fig**. 7. The excellent symmetrical source irradiation was observed for different Z-planes that is confirmed with symmetric mean absolute percentage error <0.6%. The dose rate gradient becomes very high when the detector is moved towards the vicinity of the source and decreases when the detector moves far from the source.

In addition, far from the source (> 8 cm), thanks to the high SNR (>35) and SBR (>36) of the detector, the ISD still shows significant dose rate response with respect to low dose rate, which suggests that the ISD is eligible to measure dose rate at those distal distances. Indeed, this is meaningful because the stem and background signals for ISD found to be negligible in comparison to the scintillating signal intensity, and thus the ISD could be a better alternative to the PSD and ISDs studied in [32]. Moreover, the small size and high-sensitive ISD allowed performing some measurements very close to the source (< 0.2cm) as well as far from the source (>8cm).
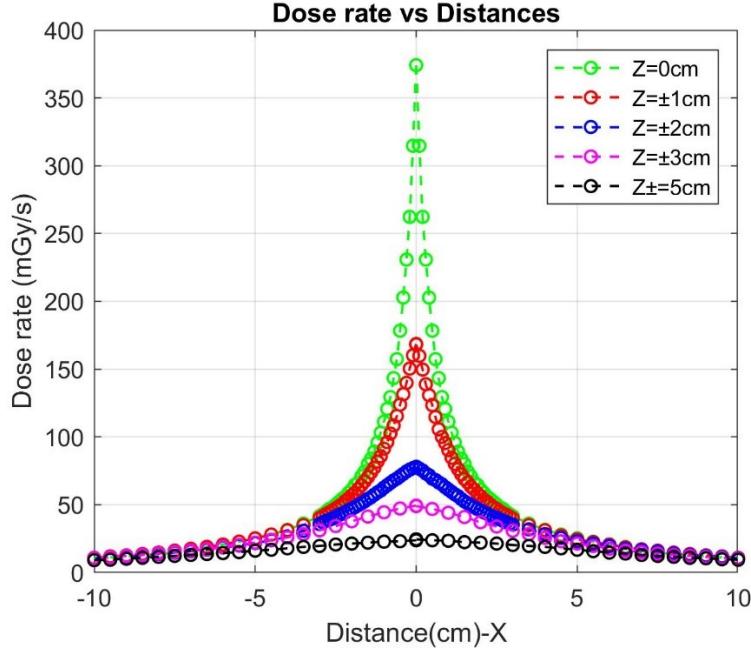
Fig. 7: Measured dose rate by the ISD as a function of source-to-detector head distance within different Z-planes [Z=0, ±1, ±2, ±3, ±5 cm]. X=0 position is considered with an accuracy of ±0.2 cm from the original source location.

3.6   Scintillation signal and system sensitivity

SNR and SBR have been quantified for ISD's output signal. SNR refers to the ratio between mean signal and signal amplitudes fluctuations under a fixed irradiation time. **Fig.** 8 (a) shows the SNR with respect to the dose rate-measurement. SNR rapidly increases with the dose rate in the range of 25 mGy/s to 50 mGy/s and then slowly increases at dose rates higher than 50 mGy/s. It exceeds 300 at a dose rate of 1000 mGy/s. A minimum SNR value of 35 has been found at the minimum dose rate investigated of 25 mGy/s at around 10cm source-to-detector distance. This means that the ISD is sensitive enough to measure dose rate above 10 cm distance from the source. SNR for the optoelectronic detector is one of the important criteria which must be above five (e.g., ROSE criteria) to achieve a proper detection performance [41]. Therefore, our detector exhibits high performance in terms of the SNR ratio.

To evaluate a proper dosimetric system behavior, SBR must be significant enough to discriminate actual scintillating signal against the background signal [42]. SBR refers to the ratio between mean signal value and mean background value under a fixed irradiation time. First, we estimated several random acquisitions without irradiation, which results in a background signal average value of 250 photons/s. Then irradiations were performed at different dose rates (so, at different source-to-detector distances), and we calculated SBR for each dose rate, as shown in **Fig**. 8(b). Because of the linear behavior of ISD optical signal with dose rate and of the constant background signal, we found a linear variation here. The minimum SBR value of 36 found for the lowest dose rate investigated 25 mGy/s. The signal standard deviation (σ_s) of the mean value known as standard uncertainty is given by GUM[43]:

$$\sigma_s = \sqrt{\frac{1}{n}\sum(x_i - \bar{x})^2}$$

370

Where x_i represents the signal intensity measured at time t_i and $\bar{x}$ is the average value of the ripple. In our case, the signal standard deviation obtained 0.03% of the total signal magnitude.
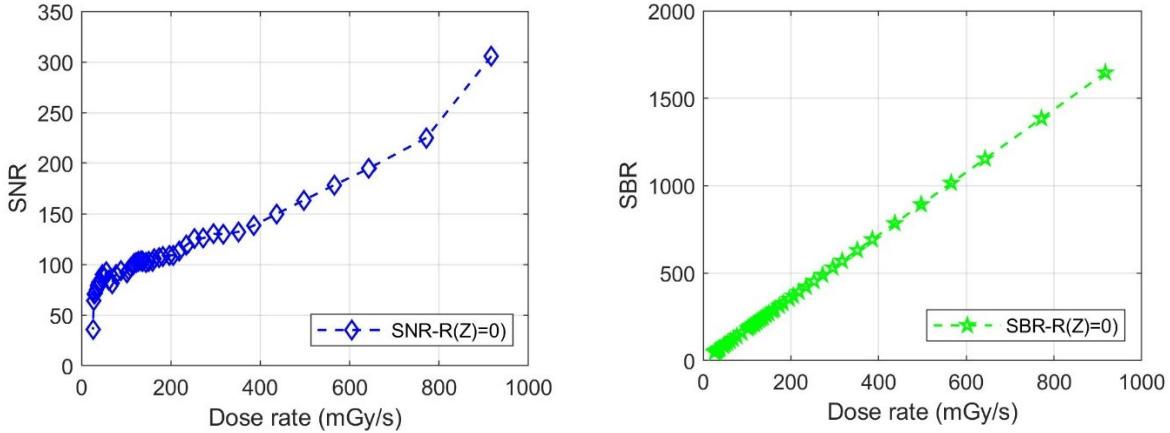

Fig. 8: (a) Signal to noise ratio (SNR) and (b) Signal to background (SBR) ration as a function of dose rate.

3.7   ISD response comparison with TG- 43 Reference

375

The ISD performance was compared with TG-43 reference dataset at Z=0 plane (symmetry plane of the capsule) and a plane far from the source (Z=5 cm). Measurements were carried out at a 0.1 cm interval with an irradiation time of 15s planned at different X-positions while the ISD signal is continuously recorded. Finally, this signal was converted to the dose rate by using the calibration
380   coefficient. **Fig**. 9(a) and 9(b) show dose rate variation as a function of detector to source distance when the detector is moving along the X-axis within two different Z-planes. All the experimental data presented here are normalized at the Z = 0, X = 1 cm, and compared to TG-43 reference dataset. The uncorrected dose rate measurements by the ISD (not corrected for energy dependence) substantially differed from the TG-43 reference dataset. This difference is more evident at far (Z=5
385   cm) distance than close to the source (Z=0) as shown in Fig. 9(a) and 9(b). The normalized raw data also show that the ISD exhibits under-response behavior nearby the source and over-response at the far distances. Moreover, at a fixed Z-depth, the higher the X distance, the lower is the discrepancy between the ISD measurements and TG-43 reference.
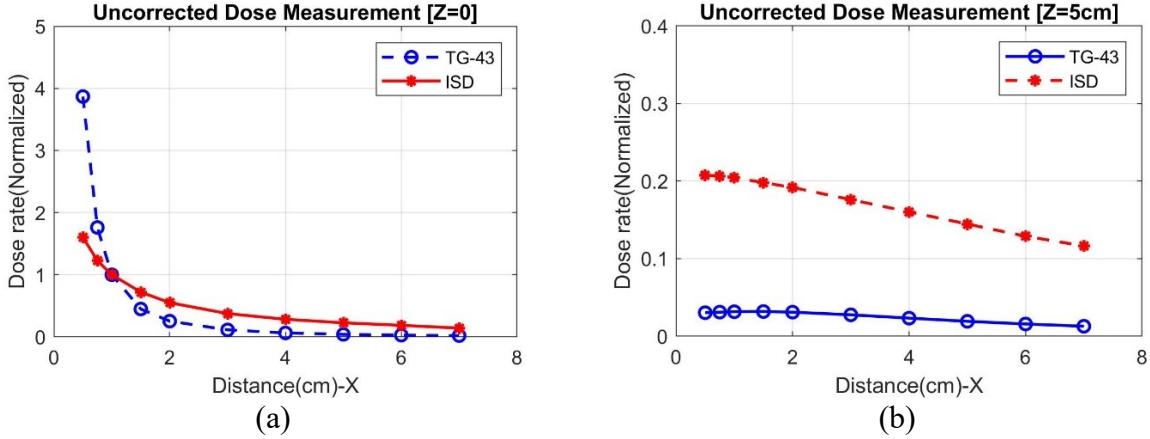
Fig. 9: Comparison of the ISD response (uncorrected) with TG-43 reference dataset for (a) Z= 0 cm and (b) Z= 5 cm.

3.8 Energy dependency and corrected dose

Fig. 10(a) shows the energy dependency of the ISD along with the radial distance at Z=0 plane. The dose response was normalized at X=1 cm. It is shown with a linear energy correction function fit. This curve highlights the detector energy dependency due to non-water equivalent detector head. Similarly, energy correction function was calculated for Z=5 plane and the respective ratio versus TG-43 is shown in **Fig**. 10(b) with a 3rd order polynomial fit. Note that, the energy dependence measurement at different Z planes could provide an energy dependent model for the ISD.
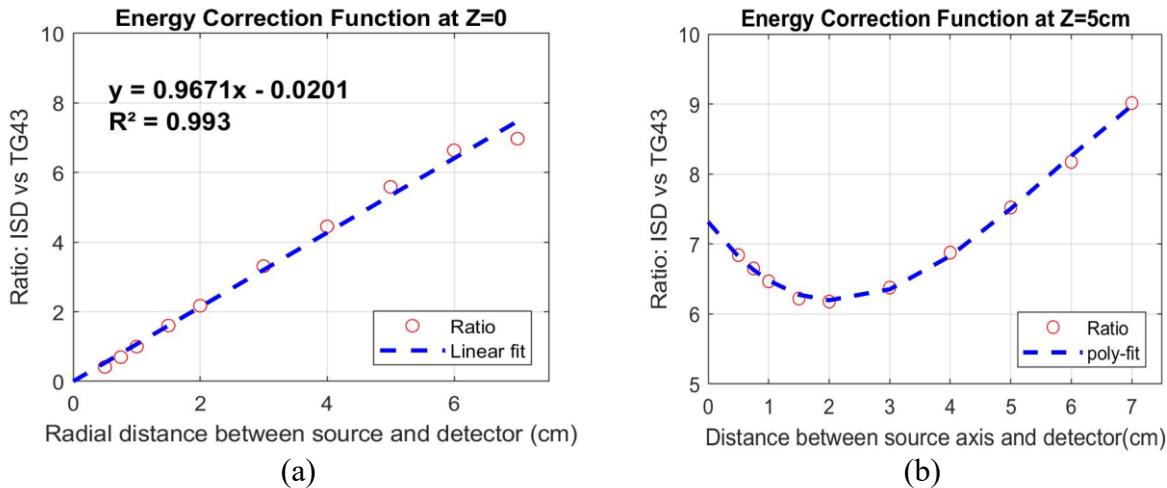

Fig. 10: (a) Energy dependence of the ISD with linear energy correction function at Z=0 plane. (b) Energy dependence of the ISD with 3rd order polynomial of energy correction function at Z=5 cm plane.

Considering energy dependence correction function shown in **Fig**. 10 for Z=0, and Z=5 cm, the ISD normalized dose rate as a function of distance are in good agreement with TG43 dataset as shown in **Fig**. 11(a) and **Fig**. 11(b). The percentage difference in the corrected dose for the Z=0 plane agrees at a minimum of 0.04%, a maximum of 3.1% with an average of 1.2% till 0.25 cm of

the source-to-detector distance. On the other hand, for Z=5 cm plane, the percentage difference agrees with TG-43 at a minimum of 0.03%, a maximum of 3.8% with an average of 1.3%. Furthermore, a slight discrepancy is still observed when the detector is very near to the source (X < 0.5 cm).

(a)   (b)
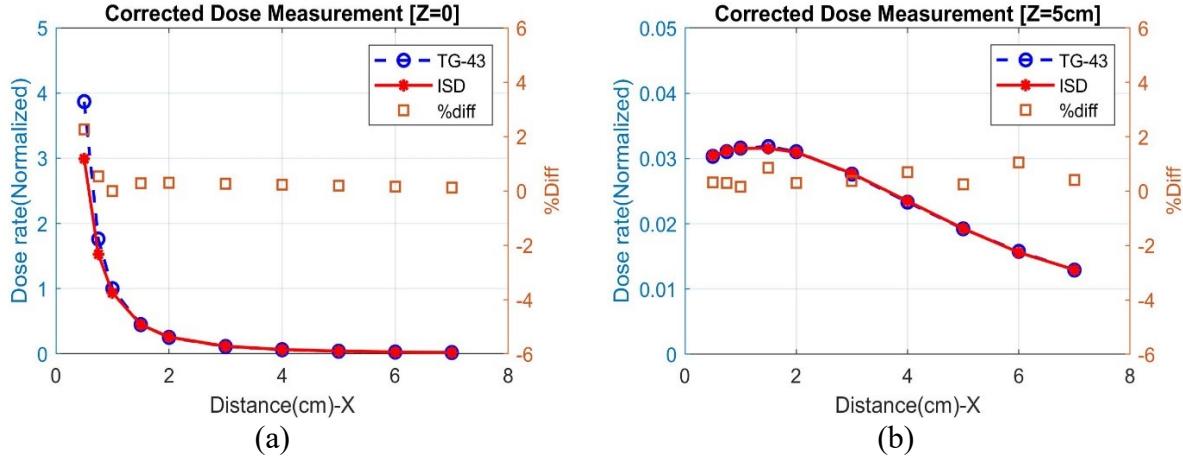
410   Fig. 11: The corrected ISD response (shown in Fig 9(a) and 9(b)) at (a) Z=0, and (b) Z=5 cm, considering the energy correction function shown in 10(a) and 10(b), respectively.

4   Discussion

This work focuses on (Zn,Cd)S:Ag scintillator-based ISD, representing several dosimetric performances tested under the Ir-192 HDR-BT source. During patient treatment, one must control
415   the accurate exposure and traveling time when the source is moved between two successive positions. Therefore, dwell time was assessed and shows good agreement with the planned dwell-time at each dwell position. The detection efficiency of the ISD was tested by measuring accurate dwell times. Higher peaks were observed at the first and last dwell positions in the needle, which is due to the larger signal difference observed between neighboring dwell positions during the
420   initial starting of irradiation and the retraction of the source at the end. The small deviation between planned and measured dwell time can be a combination of uncertainties in the dwell time determination and the afterloader positional accuracy. In addition, the uncertainties of dwell time for the first and the last dwell positions can be further improved by two detector measurement systems e.g., as shown in [44].

425   The stem signal for the ISD system is found to be negligible and in the range of background signal, which is verified for two different source-to-detector distances. This can be attributed to narrow fiber core diameter and small sensitive volume (2.9×10^{-9} cm^3). This result is consistent with our previous observations[20] in radiotherapy where STEM signal was found to be less than 1% for a beam size of 0.5x0.5 cm² at a photon energy of 6 MeV, significantly higher than photon energy in
430   BT. It is a major achievement in terms of the scintillator-based detector, where several PMMA-based ISD and PSD often require significant stem correction.

The sensitivity of the scintillator's output signal intensity was verified by determining SNR and SBR during irradiation measurement. Our point size ISD sensor presents significant SNR and SBR

even at low dose rates, i.e., far from the source and can be used to track the source even far from
its destination target. Because of the signal is proportional to the detector sensitive volume, such
performances can be achieved with conventional detectors but with a significant sensitive volume
that eventually compromises the lateral resolution of the measurement. Thus, the system can
precisely perform dose measurement with high photon collection efficiency beyond 8-10 cm
distance.

Excellent linearity with time (so with the dose) is obtained at two different source-to-ISD
distances. However, the slopes observed are different. Indeed, particles/photons generated inside
water by source local radiation have different mean free paths depending on their energy and
nature. Thus, for a given generated particle/photon, the local spectrum at the ISD head position
varies with the source to sensor distance. Furthermore, our sensor is sensitive to different kinds of
particles (e.g., electrons, low energy X-rays ranging from 2 - 200 keV, etc.), and the sensitivity for
a given particle also varies with the particle energy. This explains the reason why we could not
obtain an identical slope.

The afterglow was found to be 0.5-1% of the maximum signal irradiation for a different amount
of dose rate irradiation at different distances. Note that, this afterglow effect varies with scintillator
used. It can be easily extracted when the exact dose has to be accurately measured by using
scintillating dosimetry technique.

The dose rate comparison with TG-43 reference shows that the ISD is not an energy independent
detector. Therefore, uncorrected dose measurement shows strong discrepancies while comparing
with TG-43 reference dataset. However, considering the energy correction function, ISD achieved
acceptable performance in terms of dose measurement both in the high gradient and low gradient
dose location. A slight discrepancy is still observed when the detector is very near to the source
$(X < 0.5 \text{ cm})$, where the ISD shows under-response behavior in comparison to TG-43 dataset. This
could be due to the positional uncertainty of the detector near the source.

The reference data assume the source is as isotropic as a boundary condition. According to source
dimensions, the source capsule and pellet are cylinder-like whose axis is positioned along Z-axis.
The non-spherical source geometry cannot provide a spherical radiation diagram that is more
critical nearby the source. Accurate source radiation diagram simulation would probably give
better agreement with measurements. This point is under investigation.

5 Conclusion

In this study, an ISD based on (Zn,Cd)S: Ag scintillator coupled with silica optical fiber was tested
for brachytherapy (BT) applications. The device shows excellent performances in terms of
linearity, repeatability, signal stability, and scintillating intensities. The ISD presents an excellent
efficiency to accurately measure dwell time for several source dwell positions. The results show
that the ISD can be efficient for source tracking during BT treatment. Leveraging high SNR (> 35)
and SBR (>36) at the lowest dose rate investigated, ISD allows to accurately measure very low
dose rates far from the BT source up to 10 cm source-detector distance. Moreover, due to the point
size head, the ISD detector allows characterizing the dose rate distribution at high lateral resolution

and to measure doses very close to the source (0.1 cm distance) in the high gradient zone. Furthermore, the stem effect in the ISD measurement was negligible.

475   The ISD signal is very stable under a given dwell position and signal standard deviation remains within 0.03% of the signal magnitude.

The reference TG-43 data tend to show that measurement is valid for source-to-detector distances higher than 0.25 cm as long as an energy correction function is considered.

However, energy correction at different Z-plane does not agree with a single correction function.
480   This point is under evaluation. This study constitutes a baseline for future applications enabling dose measurements and source position tracking over a wide range of dose rate conditions. Finally, considering all the dosimetric performances, the small size ISD in this research shows that it can easily be implemented in BT needle to reduce treatment errors and thus for patient safety monitoring through a real-time dose verification system.

7 Conflict of Interest

The authors have no conflict of interest to disclose.

8 References

495   1.   Agency IAE. *Lessons learned from accidental exposures in radiotherapy.* Internat. Atomic Energy Agency; 2000.

2.   Valentin J, López PO, Andreo P, et al. Prevention of accidental exposures to patients undergoing radiation therapy. *Annals of the ICRP.* 2000;30(3).

3.   Ashton L, Cosset J, Levin V, Martinez A, Nag S. Prevention of High-Dose-Rate
500   Brachytherapy Accidents (Annals of the ICRP, ICRP Publication 97). In: Oxford: Pergamon; 2004.

4.   Richardson S. A 2-year review of recent Nuclear Regulatory Commission events: What errors occur in the modern brachytherapy era? *Practical radiation oncology.* 2012;2(3):157-163.

505   5.   Carrara M, Romanyukha A, Tenconi C, et al. Clinical application of MOSkin dosimeters to rectal wall in vivo dosimetry in gynecological HDR brachytherapy. *Physica Medica.* 2017;41:5-12.

6.   Waldhäusl C, Wambersie A, Pötter R, Georg D. In-vivo dosimetry for gynaecological brachytherapy: physical and clinical considerations. *Radiotherapy and oncology.* 2005;77(3):310-317.

7.   Brezovich IA, Duan J, Pareek PN, Fiveash J, Ezekiel M. In vivo urethral dose measurements: A method to verify high dose rate prostate treatments. *Medical physics.* 2000;27(10):2297-2301.

8.   Anagnostopoulos G, Baltas D, Geretschlaeger A, et al. In vivo thermoluminescence dosimetry dose verification of transperineal 192Ir high-dose-rate brachytherapy using CT-based planning for the treatment of prostate cancer. *International Journal of Radiation Oncology* Biology* Physics.* 2003;57(4):1183-1191.

9.   Suchowerska N, Jackson M, Lambert J, Yin YB, Hruby G, McKenzie DR. Clinical trials of a urethral dose measurement system in brachytherapy using scintillation detectors. *International Journal of Radiation Oncology* Biology* Physics.* 2011;79(2):609-615.

10.   Smith R, Taylor M, McDermott L, Haworth A, Millar J, Franich R. Source position verification and dosimetry in HDR brachytherapy using an EPID. *Medical physics.* 2013;40(11):111706.

11.   Johansen JG, Rylander S, Buus S, et al. Time-resolved in vivo dosimetry for source tracking in brachytherapy. *Brachytherapy.* 2018;17(1):122-132.

12.   Espinoza A, Beeksma B, Petasecca M, et al. The feasibility study and characterization of a two-dimensional diode array in "magic phantom" for high dose rate brachytherapy quality assurance. *Medical physics.* 2013;40(11):111702.

13.   Smith RL, Hanlon M, Panettieri V, et al. An integrated system for clinical treatment verification of HDR prostate brachytherapy combining source tracking with pretreatment imaging. *Brachytherapy.* 2018;17(1):111-121.

14.   Andersen CE, Nielsen SK, Lindegaard JC, Tanderup K. Time-resolved in vivo luminescence dosimetry for online error detection in pulsed dose-rate brachytherapy. *Medical physics.* 2009;36(11):5033-5043.

15.   Tanderup K, Beddar S, Andersen CE, Kertzscher G, Cygler JE. In vivo dosimetry in brachytherapy. *Medical physics.* 2013;40(7).

16.   Kertzscher G, Andersen CE, Tanderup K. Adaptive error detection for HDR/PDR brachytherapy: Guidance for decision making during real-time in vivo point dosimetry. *Medical physics.* 2014;41(5):052102.

17.   Ganesh T. Wrong brachytherapy treatment delivery in 100 patients. *J Med Phys.* 2014;39(2):127-130.

18.   IAEA 2000 Lessons Learned from Accidental Exposures in Radiotherapy (IAEA Safety Report Series 17) (Vienna: IAEA).

19.   Valentin J. Prevention of high-dose-rate brachytherapy accidents. ICRP Publication 97. *Annals of the ICRP.* 2005;35(2):1-51.

20. Debnath SBC, Fauquet C, Tallet A, et al. High spatial resolution inorganic scintillator detector for high-energy X-ray beam at small field irradiation. *Medical Physics.* 2020;47(3):1364-1371.

21. Alharbi M, Gillespie S, Woulfe P, McCavana P, O'Keeffe S, Foley M. Dosimetric characterization of an inorganic optical fiber sensor for external beam radiation therapy. *IEEE Sensors Journal.* 2018;19(6):2140-2147.

22. Beddar A, Mackie T, Attix F. Water-equivalent plastic scintillation detectors for high-energy beam dosimetry: I. Physical characteristics and theoretical considerations. *Physics in Medicine & Biology.* 1992;37(10):1883.

23. Beddar AS, Mackie T, Attix F. Water-equivalent plastic scintillation detectors for high-energy beam dosimetry: II. Properties and measurements. *Physics in Medicine & Biology.* 1992;37(10):1901.

24. Therriault-Proulx F, Briere TM, Mourtada F, Aubin S, Beddar S, Beaulieu L. A phantom study of an in vivo dosimetry system using plastic scintillation detectors for real-time verification of 192Ir HDR brachytherapy. *Medical physics.* 2011;38(5):2542-2551.

25. Carrara M, Cavatorta C, Borroni M, et al. Characterization of a Ce3+ doped SiO2 optical dosimeter for dose measurements in HDR brachytherapy. *Radiation measurements.* 2013;56:312-315.

26. Moutinho L, Castro I, Freitas H, et al. Scintillating fiber optic dosimeters for breast and prostate brachytherapy. Paper presented at: Optical Fibers and Sensors for Medical Diagnostics and Treatment Applications XVII2017.

27. Lambert J, Nakano T, Law S, Elsey J, McKenzie DR, Suchowerska N. In vivo dosimeters for HDR brachytherapy: A comparison of a diamond detector, MOSFET, TLD, and scintillation detector. *Medical physics.* 2007;34(5):1759-1765.

28. Archambault L, Beddar AS, Gingras L, Roy R, Beaulieu L. Measurement accuracy and Cerenkov removal for high performance, high spatial resolution scintillation dosimetry. *Medical physics.* 2006;33(1):128-135.

29. Andersen CE. Fiber-coupled Luminescence Dosimetry in Therapeutic and Diagnostic Radiology. Paper presented at: AIP Conference Proceedings2011.

30. Therriault-Proulx F, Beddar S, Briere TM, Archambault L, Beaulieu L. Removing the stem effect when performing Ir-192 HDR brachytherapy in vivo dosimetry using plastic scintillation detectors: A relevant and necessary step. *Medical physics.* 2011;38(4):2176-2179.

31. Fontbonne J, Iltis G, Ban Ga, et al. Scintillating fiber dosimeter for radiation therapy accelerator. *IEEE Transactions on Nuclear Science.* 2002;49(5):2223-2227.

32. Kertzscher G, Beddar S. Inorganic scintillation detectors for 192Ir brachytherapy. *Physics in Medicine & Biology.* 2019;64(22):225018.

33. Kertzscher G, Beddar S. Inorganic scintillator detectors for real-time verification during brachytherapy. Paper presented at: Journal of Physics: Conference Series2017.

585   34.   Yen WM, Weber MJ. *Inorganic phosphors: compositions, preparation and optical properties.* CRC press; 2004.

35.   Knoll GF. *Radiation detection and measurement.* John Wiley & Sons; 2010.

36.   Wootton L, Beddar S. Temperature dependence of BCF plastic scintillation detectors. *Physics in Medicine & Biology.* 2013;58(9):2955.

590   37.   Johansen J, Kertzscher G, Jørgensen E, et al. Dwell time verification in brachytherapy based on time resolved in vivo dosimetry. *Physica Medica.* 2019;60:156-161.

38.   Kertzscher G, Beddar S. Inorganic scintillator detectors for real-time verification during brachytherapy. Paper presented at: Journal of Physics: Conference Series2017.

39.   Perez-Calatayud J, Ballester F, Das RK, et al. Dose calculation for photon-emitting brachytherapy sources with average energy higher than 50 keV: report of the AAPM and ESTRO. *Medical physics.* 2012;39(5):2904-2929.

595

40.   Meigooni A, Meli J, Nath R. Influence of the variation of energy spectra with depth in the dosimetry of 192Ir using LiF TLD. *Physics in Medicine & Biology.* 1988;33(10):1159.

41.   Bushberg JT, Boone JM. *The essential physics of medical imaging.* Lippincott Williams & Wilkins; 2011.

600

42.   Linares Rosales HM, Duguay-Drouin P, Archambault L, Beddar S, Beaulieu L. Optimization of a multipoint plastic scintillator dosimeter for high dose rate brachytherapy. *Medical physics.* 2019;46(5):2412-2421.

43.   Guide I. Uncertainty of Measurement–Part 3: Guide to the Expression of Uncertainty in Measurement. *International Organization for Standardization, Geneva, Switzerland.* 1995.

605

44.   Guiral P, Ribouton J, Jalade P, et al. Design and testing of a phantom and instrumented gynecological applicator based on GaN dosimeter for use in high dose rate brachytherapy quality assurance. *Medical physics.* 2016;43(9):5240-5251.